Scripta Materialia 202 (2021) 113991

Contents lists available at ScienceDirect

Scripta Materialia

journal homepage: www.elsevier.com/locate/scriptamat

Direct numerical analyses of nanoscale thermal transport near MgO edge dislocations

Wataru Sekimoto[a], Susumu Fujii[a,b], Masato Yoshiya[a,b,c,*]

[a] Division of Materials and Manufacturing Science, Osaka University, 2-1 Yamadaoka, Suita, Osaka 565-0871, Japan.
[b] Nanostructures Research Laboratory, Japan Fine Ceramics Center, 2-4-1 Mutsuno, Atsuta, Nagoya 456-8587, Japan.
[c] Anisotropic Design & Additive Manufacturing Research Center, Osaka University, 2-1 Yamadaoka, Suita, Osaka 565-0871, Japan

ARTICLE INFO

Article history:
Received 28 February 2021
Revised 1 May 2021
Accepted 8 May 2021

Keywords:
Dislocation
Thermal conductivity
Materials design
Molecular dynamics
Anisotropy

ABSTRACT

We report numerical analyses to examine the impact of edge dislocation onto phonon thermal conduction in its vicinity. Two types of edge dislocations, one with open core and another with densely-packed core, show different magnitude of suppression of thermal conductivity across dislocation lines, more than crystallographic anisotropy. It is also found that small density of dislocations effectively scatters phonons lowering thermal conductivity while higher density of dislocations is less effective to suppress thermal conduction. Detailed analyses on bond strains and atomic vibrational states indicated that, while linear dependence of atomic thermal conductivity is found when bond strain is small as in elastic strain field, non-linear/anharmonic dependence of atomic thermal conductivity emerges for the highly strained and under-coordinated atoms at the cores. A combination of these leads to remarkable suppression in thermal conductivity at non-arrayed dislocations even if atoms are positioned away from dislocation core.

Extensive studies of dislocations for many decades have enabled us to go further toward nanostructures. Those include pioneering studies Hall and Petch for hardening [1,2], which are paralleled by theoretical studies by Peierls, Cottrell, Read and Shockley and Eshelby et al., to name just a few [3–6], followed by transmission electron microscopy observation [7]. All of these have facilitated in-depth understanding of structure-property relationships mainly of mechanical properties even for complicated materials including nanostructured materials in terms of nucleation or transient dislocations [8–13], in conjunction with computational atomistic modeling techniques including those by molecular dynamics simulations with classical force fields [14–16] and *ab initio* calculations [17–21], and recently also by machine learning [22].

Attempts have been made to exploit dislocations for more diverse properties other than mechanical properties. The roles of dislocations on colossal pipe diffusion [23–25] and epitaxial growth are well known. However, most of them often remain to remove detrimental effects of dislocations or make them benign against the target properties of materials [26–29]. Recently, a new strategy for molecular decoding by utilizing dislocation is proposed [30]. With an aid of pipe diffusion along dislocations, conducting nanowires are realized in an insulator material [31]. Photo-assisted/impeded plastic deformation is experimentally demonstrated for a semiconductor material [32], which can be attributed to interplay between photons, electrons and dislocations [33].

More successful results have been obtained for possible applications for thermoelectrics where conflicting demands for two transport properties of quantum waves persist. One of pioneering study reported that increased dislocation density together with grain boundaries (GBs) and vacancies by high pressure torsion (HPT) successfully suppress phonon thermal conductivity, thereby increasing the thermoelectric conversion efficiency [34]. Misfit dislocations and arrays of dislocations, or low angle GBs, are found to be effective to suppress thermal conductivity (especially when dopant segregation occurs), while minimizing detrimental impact on electronic counterparts [35–39] . Following those geometrically-necessary (GN) dislocations, it has been experimentally confirmed that statistically-stored (SS) dislocations also play pivotal role for controlling phonon thermal conductivity [40,41], which opens up a new way to maximizing the thermoelectric figure of merit through careful tailoring of microstructures or nanostructures. However, interpretation of those favorable results rely on conventional analytical theories [42,43] proposed many decades ago, while large deviation from Matthiessen's sum rule is reported [44].

A pioneering work by Klemens proposed phonon scattering by dislocations based on a discrete lattice model with nonlinear elas-

* Corresponding author.
E-mail address: yoshiya@mat.eng.osaka-u.ac.jp (M. Yoshiya).

https://doi.org/10.1016/j.scriptamat.2021.113991

ticity theory where dislocations are described by an array of vacancies with elastic strain field around it [42,43], which remain unchanged in updates for nanostructures by Cahill et al [44,45]. In contrast, Fujii et al. recently demonstrated that thermal conductivity near arrayed GN dislocations, or low angle tilt GBs, depends highly on the atomic structures of dislocations, where a dislocation core with lower number density of atoms is more effective for reducing thermal conductivity [46]. In addition, they also revealed that even small bond strains near GN dislocations can dramatically reduce thermal conductivity, through the development of a model that predicts GB thermal conductivity from their atomic structures [47].

It is expected, however, that isolated SS dislocations introduce different impact on thermal conduction in its vicinity compared with the ones by GBs where strain fields of arrayed GN dislocations can be cancelled out. Lack of precise understanding of the influence of SS dislocations on phonon thermal conduction impedes further attempts by experiments as introduction or annihilation of SS dislocation through thermal materials processing inevitably accompanies rapid vacancy diffusion and slow grain growth. Thus, in this study, numerical analyses are performed to understand the roles that SS dislocation play on thermal conduction using molecular dynamics.

To evaluate and analyze thermal conductivity, we used perturbed molecular dynamics method [48]. For this purpose we have added custom-written codes to LAMMPS package [49]. Advantages of using it in this study over other methods includes direct quantifications of thermal conductivity based solely on motions of atoms, without artificial phonon scatterings which complicates the analyses or any assumption regarding phonon scatterings. In this method, thermal conductivity is obtained as a function of temporal average of microscopic heat flux, **J**, which is given by

$$\mathbf{J} = \sum_i \mathbf{J}_i = \sum_i \frac{1}{2V}\left[\left\{ m_i \mathbf{v}_i^2 + \sum_j \phi_{ij} \right\}\mathbf{I}\cdot\mathbf{v}_i - \sum_j \left(\mathbf{F}_{ij}\cdot\mathbf{v}_i\right)\mathbf{r}_{ij}\right] \quad (1)$$

where m_i and $\mathbf{v}_i$ are mass and velocity of atom i, ϕ_{ij} denotes internal energy determined by interatomic interaction, V is volume of a supercell, $\mathbf{F}_{ij}$ is a force exerted from atom j to atom i, $\mathbf{r}_{ij} = \mathbf{r}_j - \mathbf{r}_i$ with $\mathbf{r}_i$ being a position of atom i, and $\mathbf{I}$ is a unit tensor of second rank. Since the summation is taken over all the atoms, atomic heat flux, $\mathbf{J}_i$, can be unambiguously determined [48,50]. Phonon thermal conductivity is then given by,

$$\boldsymbol{\kappa}_{\mathrm{ph}} = \sum_i \boldsymbol{\kappa}_i = \sum_i \frac{1}{\mathbf{F}_{\mathrm{ext}} T} \lim_{t\to\infty} \langle \mathrm{J}_i \rangle_t \quad (2)$$

where T is target temperature of a system. In this method, small amount of perturbation which is determined by current instantaneous microscopic heat flux is added to the equation of motion. Its magnitude and direction are determined by an adjustable parameter, $\mathbf{F}_{\mathrm{ext}}$, to the extent it generates non-zero heat flux within the linear response regime. Dependence on it disappears by dividing temporal average of heat flux by it. Because of this relationship between overall thermal conductivity and microscopic heat flux of each atom, contributions of each atom to overall thermal conductivity, which hereafter is referred to as atomic thermal conductivity, can be uniquely decomposed to. This enables mapping of atomic thermal conductivity around dislocations [46,48,50,51]. As shown in Eq. (2), atomic thermal conductivities are extensive variables but can be readily converted to intensive variables by dividing the heat flux (Eq. (1)) by the volume per atom instead of the volume of a supercell [51].

In this study, rock-salt structured MgO is chosen as a model material. Taking into account the fact that the difference in ionic radii between O and Mg is greater than atomic radii of Fe and C, this crystal is actually formed by FCC sublattice of large O ions with small Mg ions at its octahedral sites, in common with other variety of oxides and also with metals. This enables comparison with them and extension of findings to those materials. Interatomic bonding between Mg and O is highly ionic and non-directional, and thus simple classical pair-wise Buckingham potential is used [52]. This yields thermal conductivity of 119.2 W/mK for a single crystal. The overestimation of thermal conductivity compared with the experimental value (~ 50 W/mK [53,54]) can be mainly attributed to the effects of isotopes, impurities and pores in experimental samples [46]. We intentionally neglect these effects to focus on the relative changes of thermal conductivity caused solely by dislocations. In addition, the group velocities of phonons in MgO are overestimated with the employed Buckingham potential compared with that obtained by *ab initio* calculations (see Figs. S1 and S2 in Supplementary Materials). However, the shape of phonon dispersions is well represented with this potential, and thus it is plausible to assume that phonon transport and its scattering mechanism is also well represented.

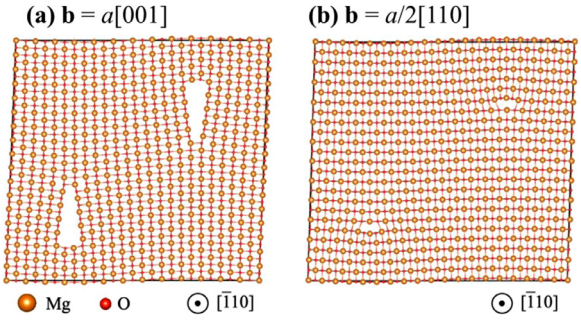

Fig. 1. Edge dislocation models with the Burgers vectors of (a) a[001] and (b) $a/2$[110]. The dislocation densities are about 7×10^{16} m^{-2}.

Supercells with dislocations are constructed as follows: At first two crystal slabs oriented along dislocation line, one with an extra half plane and one without it, are adjoined. The two adjoined slabs with a dislocation in each are then adjoined to form a supercell such that Burgers vectors of two edge dislocations are antiparallel and two edge dislocations are placed at farthest and most stable positions at an angle 45 degrees between two dislocation cores according to the Peach-Koehler equation. For each type of dislocation, models were constructed with different dislocation densities ρ up to about 7×10^{16} m^{-2}.

The dimensions of each supercell were determined under a constant pressure condition (1.013×10^5 Pa) by molecular dynamics for 100 ps at 300 K. Thermal equilibrium without the perturbation after 400 ps and steady state with the perturbation after 3 ns are achieved under a constant volume condition using Nosé-Hoover thermostat. Then, thermal conductivity was measured with the perturbation for 7 ns with reliable statistical accuracy. Multiple $\mathbf{F}_{\mathrm{ext}}$ are used to ensure that the system stays within linear response regime and for statistical accuracy of independently measured thermal conductivity including atomic thermal conductivity.

In this study, we investigated the impact of two different edge dislocations with a line vector $\mathbf{t} = [\bar{1}10]$ on the phonon thermal conductivity. One has an open dislocation core with a Burgers vector $\mathbf{b} = a$[001] and the other has a densely packed core with $\mathbf{b} = a/2$[110] (Fig. 1), where a corresponds to the lattice constant of MgO. Hereafter, these dislocations are referred to as [001] and 1/2[110] dislocations, respectively. The constructed cell for [001] dislocation with $\rho \cong 7 \times 10^{16}$ m^{-2} has the dimensions of $53.3 \times 50.5 \times 20.8$ Å and contains 5880 atoms. Here, we focus on the thermal conduction across dislocation lines, because the suppression of thermal conductivity is much significant compared with those along the dislocation lines (see Fig. S3 in Supplementary Materials for details).

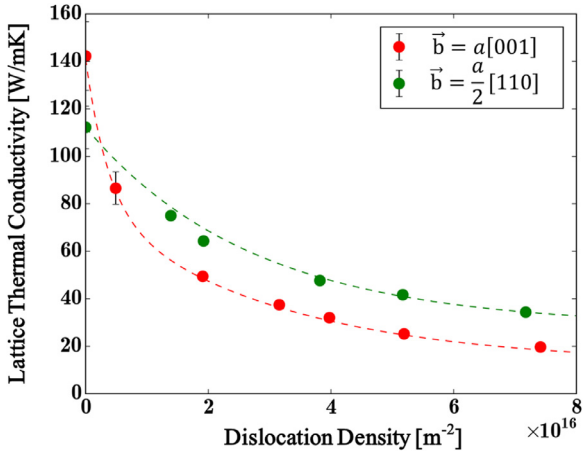

Fig. 2. Lattice thermal conductivity as a function of dislocation density for two edge dislocations with $\mathbf{b} = a[001]$ and $a/2[110]$.

Fig. 2 compares the dislocation-density dependence of phonon thermal conductivity between [001] and 1/2[110] dislocations. Thermal conductivity with no dislocations ($\rho = 0$) was also plotted in the figure to show the orientation dependence of single crystalline thermal conductivity. Introducing small density of dislocations steeply reduced the thermal conductivity, followed by gradual decreases with increasing ρ. The reduction of thermal conductivity is more evident for [001] dislocation with the open cores, as the thermal conductivity is always lower than that of 1/2[110] dislocation despite the higher single crystalline thermal conductivity. Especially, with the very high ρ of about 7×10^{16} m^{-2}, the thermal conductivity of 1/2[110] dislocation model is almost doubled that of [001] dislocation model. This indicates that open dislocation cores, which has lower atomic number density and more ruptured bonds, are more effective to decrease the thermal conductivity, while densely packed cores are less influential. This trend is consistent with the results of the low-angle tilt GBs (arrayed GN dislocations).

To investigate the suppression mechanism of thermal conduction in the vicinity of the dislocation cores, we calculated atomic thermal conductivities for $\rho \cong 7 \times 10^{16}$ m^{-2}, and projected them to a two dimensional plane (Fig. 3a). In both dislocation models, atomic thermal conductivities were substantially decreased not only in the vicinity of dislocation cores but also in the region away from them; the maximum of atomic thermal conductivities is 43 W/mK in 1/2[110] dislocation model, which is almost one thirds of the single crystalline thermal conductivity of MgO (119.2 W/mK) calculated in this study. The [001] dislocation model exhibits much lower atomic thermal conductivities at any region compared to the 1/2[110] model. These results demonstrate that the influence of dislocation cores on thermal transport is spatially widespread, especially when the dislocation core has an open structure.

Fig. 3a also shows that atomic thermal conductivities are relatively high at the region including an extra half plane and low between the dislocation cores, implying that the strain fields near the dislocation cores modify the thermal transport at the nanoscale. Thus, we estimated the bond strain of each atom according to the following definition:

$$\varepsilon_i = \frac{\sum_i^{CN_i} l_{ij} - l_{\mathrm{bulk}} \times CN_i}{l_{\mathrm{bulk}} \times CN_i}, \tag{3}$$

where ε_i is the bond strain of atom i, CN_i is the coordination number, l_{ij} and l_{bulk} are the distances from atom i to the nearest neighbor atom j in the dislocation model and the bulk model, respectively. The two-dimensional maps of the bond strains are plotted in Fig. 3b. A typical strain field pair was found for both dislocations, where the extra half plane induced the compressive strain while the other side was subjected to the tensile strain. Comparing Fig. 3a and 3b, it can be seen that there is a strong correlation between the bond strains and atomic thermal conductivities, i.e., thermal conductivity is relatively large when the bonds are compressed, and vice versa. Indeed, our separate calculations on the uniformly compressed or expanded MgO single crystals revealed that the compressive (tensile) strains increase (decrease) the lattice thermal conductivity significantly (See Fig. S4 in Supplementary Materials).

Fig. 3c displays the differences in the mean square displacement (MSD) of each atom compared to the bulk MgO relative to its average over all directions. The MSD values correspond to the amplitudes of atomic vibrations. As seen from the comparison of Fig. 3b and 3c, the bond strain is correlated well with the MSD in both dislocation models, indicating that compressed bonds lead to the stronger interactions Mg and O ions and thereby smaller MSD, and vice versa. The bond strain apparently modifies the dynamical behavior of atoms, disrupting their collective motions and consequently reducing the thermal conductivity. It was also found from Fig. 3c that the MSD values significantly increased for the under-coordinated atoms at the cores and their neighboring atoms. These atoms exhibit very low atomic thermal conductivities as shown in Fig. 3a, due to the largely anharmonic vibrations induced by the coordination deficiencies at the cores.

To gain a more quantitative understanding, the atomic thermal conductivities are plotted as a function of the bond strain in Fig. 4, by taking the average of them for each 0.5% of bond strain ε. Only fully coordinated atoms (CN = 6) were included in this figure to separate the impacts of bond strains and coordination deficiencies. The difference in atomic thermal conductivities between [001] and 1/2[110] models is as large as 15.3 W/mK at $\varepsilon = 0\%$, demonstrating the large scattering effect of the open core structure. In both [001] and 1/2[110] dislocations, atomic thermal conductivities linearly decreased as the bond strain increased, especially in the range of -0.5% $\leq \varepsilon \leq$ 0.5%. The magnitudes of decreases are 5.1 W/mK for [001] dislocation and 7.6 W/mK for 1/2[110] dislocation, respectively, which are non-negligible considering their overall thermal conductivities of 20 and 34 W/mK. These results quantitatively showed that the suppression of thermal conductivity can be attributed not only to the scattering by the cores but also to the strain field in its vicinity.

In addition, non-linear/anharmonic influence of bond strains onto atomic thermal conductivity is quantitatively demonstrated in Fig. 4. The compressive strains with $\varepsilon <$ -0.5% did not increase the atomic thermal conductivities, probably due to the significant bond strains near the dislocation cores that is non-uniform not only in lengths but also in angles. On the other hand, with larger tensile strains, atomic thermal conductivities continued to decrease in 1/2[110] model, while they plateaued out in [001] model. The large tensile strains would be less effective near the open core structure because the thermal conductivity is already significantly reduced. With the large tensile strain of $\varepsilon = 1.5\%$, atomic thermal conductivities are as low as 17.9 $\pm$ 2.8 W/mK for [001] dislocation model and 21.9 $\pm$ 2.7 W/mK for 1/2[110] dislocation model, respectively. The value for 1/2[110] dislocation model is comparable to that of the under-coordinated atoms at the dislocation core (21.2 $\pm$ 4.7 W/mK), indicating the large impact of bond strains. On the other hand, the under-coordinated atoms in [001] dislocation model exhibit much lower atomic thermal conductivity of 11.2 $\pm$ 6.2 W/mK compared with that of the fully coordinated atoms. The different trends between two dislocation cores are due to the different magnitude of anharmonic vibrations as suggested in the results of MSD (Fig. 3c): the under-coordinated atoms at the [001] dislocation core vibrates with larger MSD values (larger am-

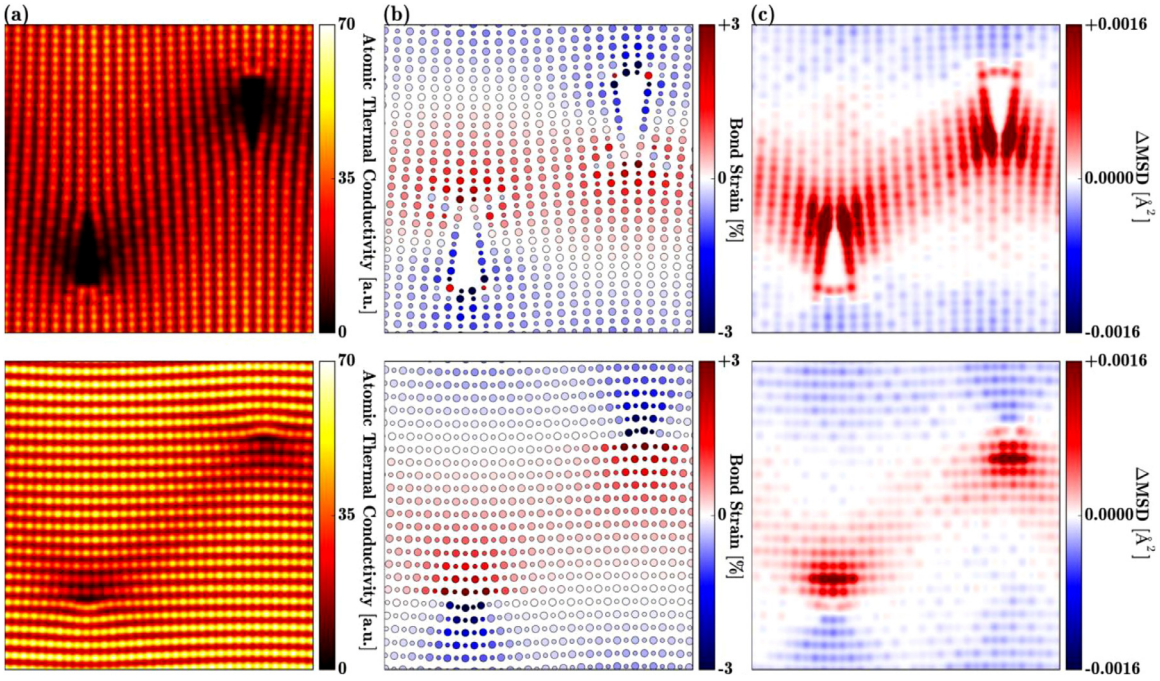

Fig. 3. Two-dimensional maps of (a) atomic thermal conductivities, (b) bond strains, and (c) differences in mean square displacements ΔMSD, compared to the bulk MgO. The upper and lower panels show the results of two edge dislocations with **b** = a[001] and a/2[110].

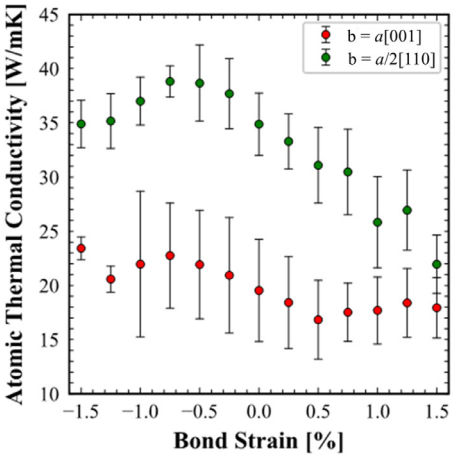

Fig. 4. Atomic thermal conductivities as a function of bond strain for two edge dislocations with **b** = a[001] and a/2[110].

plitudes) than those at the 1/2[110] dislocation core. These results demonstrated that nanoscale thermal conduction near dislocations is highly dependent on the local distortion such as bond strains and coordination deficiencies induced by the different types of the core structures.

In summary, we performed numerical analyses of phonon thermal conduction in the vicinity of edge dislocations in MgO by means of perturbed molecular dynamics. The main factors in disturbing the collective vibrations of atoms are found to be the dislocation core structures with coordination deficiencies and linear/nonlinear bond strains, beyond the simple description as one-dimensional obstacles and associated linear-elastic strain field deduced earlier. These then suppress atomic thermal conductivity, not only of atoms in the vicinity of the dislocation core but also of atoms away from the dislocation core. As a consequence, overall thermal conduction is suppressed by the dislocations, and dependence of thermal conductivity on dislocation density becomes nonlinear.

Author contributions

WS performed theoretical calculations and analyses. SF and MY advised on the calculations and analyses. MY and SF designed the study. All authors discussed the results and wrote the manuscript.

Declaration of Competing Interest

The authors declare no competing financial interest.

Acknowledgments

This study is in part supported by Grant-in-Aid for Scientific Research on Innovative Areas 'New Materials Science on Nanoscale Structures and Functions of Crystal Defect Cores' [Grant Number: JP19H05786]. SF was also supported by Grant-in-Aid for Scientific Research [Grant Numbers: JP20H05195 and JP20K15034]. MY was also supported by Grant-in-Aid for Scientific Research [Grant Number: JP20K05062].

Supplementary materials

Supplementary material associated with this article can be found, in the online version, at doi:10.1016/j.scriptamat.2021.113991.

References

[1] E.O. Hall, Proc. Phys. Soc. Sect. B 64 (1951) 747–753.
[2] N.J. Petch, J. Iron Steel Inst. 174 (1953) 25–28.
[3] R. Peierls, Proc. Phys. Soc. 52 (1940) 34–37.
[4] A.H. Cottrell, B.A. Bilby, Proc. Phys. Soc. Sect. A 62 (1949) 49–62.
[5] W.T. Read, W. Shockley, Phys. Rev. 78 (1950) 275–289.
[6] J.D. Eshelby, W.T. Read, W. Shockley, Acta Metall. 1 (1953) 251–259.
[7] P.B. Hirsch, R.W. Horne, M.J. Whelan, Philos. Mag. 1 (1956) 677–684.
[8] R.J. Asaro, S. Suresh, Acta Mater. 53 (2005) 3369–3382.
[9] S. Suresh, J. Li, Nature 456 (2008) 716–717.

[10] P. Gu, B.K. Kad, M. Dao, Scr. Mater. 62 (2010) 361–364.
[11] P. Gu, M. Dao, R.J. Asaro, S. Suresh, Acta Mater. 59 (2011) 6861–6868.
[12] L.Y. Chen, M. He, J. Shin, G. Richter, D.S. Gianola, Nat. Mater. 14 (2015) 707–713.
[13] J. Li, Nat. Mater. 14 (2015) 656–657.
[14] J. Wang, R.G. Hoagland, J.P. Hirth, A. Misra, Acta Mater. 56 (2008) 5685–5693.
[15] T. Zhu, J. Li, A. Samanta, A. Leach, K. Gall, Phys. Rev. Lett. 100 (2008) 025502.
[16] K. Dang, D. Bamney, L. Capolungo, D.E. Spearot, Acta Mater. 185 (2020) 420–432.
[17] G.P.M. Leyson, L.G. Hector, W.A. Curtin, Acta Mater. 60 (2012) 3873–3884.
[18] D. Rodney, L. Ventelon, E. Clouet, L. Pizzagalli, F. Willaime, Acta Mater. 124 (2017) 633–659.
[19] G. Hachet, L. Ventelon, F. Willaime, E. Clouet, Acta Mater. 200 (2020) 481–489.
[20] L. Casillas-Trujillo, D. Gambino, L. Ventelon, B. Alling, Phys. Rev. B 102 (2020) 094420.
[21] A. Togo, I. Tanaka, Scr. Mater. 108 (2015) 1–5.
[22] A. Pandey, R. Pokharel, Scr. Mater. 193 (2021) 1–5.
[23] R.L. Tallman, E.A. Gulbransen, Nature 218 (1968) 1046–1047.
[24] A. Pertsinidis, X.S. Ling, Nature 413 (2001) 147–150.
[25] K. Otsuka, A. Kuwabara, A. Nakamura, T. Yamamoto, K. Matsunaga, Y. Ikuhara, Appl. Phys. Lett. 82 (2003) 877–879.
[26] S.F. Chichibu, A. Uedono, T. Onuma, B.A. Haskell, A. Chakraborty, T. Koyama, P.T. Fini, S. Keller, S.P. DenBaars, J.S. Speck, U.K. Mishra, S. Nakamura, S. Yamaguchi, S. Kamiyama, H. Amano, I. Akasaki, J. Han, T. Sota, Nat. Mater. 5 (2006) 810–816.
[27] D. Liang, J.E. Bowers, Nat. Photonics 4 (2010) 511–517.
[28] P. Yan, J. Zheng, M. Gu, J. Xiao, J.-G. Zhang, C.-M. Wang, Nat. Commun. 8 (2017) 14101.
[29] S.D. Lester, F.A. Ponce, M.G. Craford, D.A. Steigerwald, Appl. Phys. Lett. 66 (1995) 1249–1251.
[30] Y. Takashima, V.M. Martínez, S. Furukawa, M. Kondo, S. Shimomura, H. Uehara, M. Nakahama, K. Sugimoto, S. Kitagawa, Nat. Commun. 2 (2011) 168.
[31] A. Nakamura, K. Matsunaga, J. Tohma, T. Yamamoto, Y. Ikuhara, Nat. Mater. 2 (2003) 453–456.
[32] Y. Oshima, A. Nakamura, K. Matsunaga, Science 360 (2018) 772–774.
[33] K. Matsunaga, S. Hoshino, M. Ukita, Y. Oshima, T. Yokoi, A. Nakamura, Acta Mater. 195 (2020) 645–653.
[34] G. Rogl, D. Setman, E. Schafler, J. Horky, M. Kerber, M. Zehetbauer, M. Falmbigl, P. Rogl, E. Royanian, E. Bauer, Acta Mater. 60 (2012) 2146–2157.
[35] S.-H. Lo, J. He, K. Biswas, M.G. Kanatzidis, V.P. Dravid, Adv. Funct. Mater. 22 (2012) 5175–5184.
[36] S. Il Kim, K.H. Lee, H.A. Mun, H.S. Kim, S.W. Hwang, J.W. Roh, D.J. Yang, W.H. Shin, X.S. Li, Y.H. Lee, G.J. Snyder, S.W. Kim, Science 348 (2015) 109–114.
[37] H. Zhao, B. Cao, S. Li, N. Liu, J. Shen, S. Li, J. Jian, L. Gu, Y. Pei, G.J. Snyder, Z. Ren, X. Chen, Adv. Energy Mater. 7 (2017) 1700446.
[38] H. Mun, K.H. Lee, S.J. Yoo, H.-S. Kim, J. Jeong, S.H. Oh, G.J. Snyder, Y.H. Lee, Y.-M. Kim, S.W. Kim, Acta Mater. 159 (2018) 266–275.
[39] N. Goel, E.B. Webb, A. Oztekin, J.M. Rickman, S. Neti, J. Appl. Phys. 118 (2015) 115101.
[40] V. Karthikeyan, C.M. Arava, M.Z. Hlaing, B. Chen, C.H. Chan, K.-H. Lam, V.A.L. Roy, Scr. Mater. 174 (2020) 95–101.
[41] Z. Chen, Z. Jian, W. Li, Y. Chang, B. Ge, R. Hanus, J. Yang, Y. Chen, M. Huang, G.J. Snyder, Y. Pei, Adv. Mater. 29 (2017) 1606768.
[42] P.G. Klemens, Proc. Phys. Soc. Sect. A 68 (1955) 1113–1128.
[43] P.G. Klemens, in: F. Seitz, D. Turnbull (Eds.), Solid State Phys., Academic Press, 1958, pp. 1–98.
[44] D.G. Cahill, P.V. Braun, G. Chen, D.R. Clarke, S. Fan, K.E. Goodson, P. Keblinski, W.P. King, G.D. Mahan, A. Majumdar, H.J. Maris, S.R. Phillpot, E. Pop, L. Shi, Appl. Phys. Rev. 1 (2014) 011305.
[45] D.G. Cahill, W.K. Ford, K.E. Goodson, G.D. Mahan, A. Majumdar, H.J. Maris, R. Merlin, S.R. Phillpot, J. Appl. Phys. 93 (2003) 793–818.
[46] S. Fujii, T. Yokoi, M. Yoshiya, Acta Mater 171 (2019) 154–162.
[47] S. Fujii, T. Yokoi, C.A.J. Fisher, H. Moriwake, M. Yoshiya, Nat. Commun. 11 (2020) 1854.
[48] M. Yoshiya, A. Harada, M. Takeuchi, K. Matsunaga, H. Matsubara, Mol. Simul. 30 (2004) 953–961.
[49] S. Plimpton, J. Comput. Phys. 117 (1995) 1–19.
[50] M. Tada, M. Yoshiya, H. Yasuda, Proc. Phys. Soc. Sect. A 68 (1955) 1113–1128.
[51] S. Fujii, M. Yoshiya, J. Electron. Mater. 45 (2016) 1217–1226.
[52] J.D. Gale, J. Chem. Soc. Faraday Trans. 93 (1997) 629–637.
[53] A.M. Hofmeister, Phys. Chem. Miner. 41 (2014) 361–371.
[54] D.A. Dalton, W.-P. Hsieh, G.T. Hohensee, D.G. Cahill, A.F. Goncharov, Sci. Rep. 3 (2013) 2400.